LA-UR -87-4218

CONF-880654--5

Los Alamos National Laboratory is operated by the University of California for the United States Department of Energy under contract W-7405-ENG-36

LA-UR--87-4218

DE88 004289

TITLE MICROSTRUCTURAL EFFECTS IN STATIC AND DYNAMIC NUMERICAL EXPERIMENTS

AUTHOR(S) BRUCE C. TRENT, ESS-5

SUBMITTED TO 29th U. S. Symposium on Rock Mechanics
University of Minnesota, Minneapolis, MN
June 13-15, 1988

DISCLAIMER

Los Alamos National Laboratory
Los Alamos, New Mexico 87545

Microstructural Effects in Static and Dynamic Numerical Experiments

Bruce C. Trent
Los Alamos National Laboratory

ABSTRACT: A numerical analysis of cemented granular material has been performed in order to better understand the relationship between the individual components of a rock matrix and the macroscopic constitutive response. A distinct element code was modified to allow interparticle bonding by incorporating appropriate elastic relationships. A modified Griffith criterion was utilized to initiate fracture within individual bonds. A number of quasi-static and dynamic numerical experiments are presented which show that realistic macroscopic behavior may be obtained without the use of phenomenological formulations such as plasticity.

1 INTRODUCTION

As computer programs become more sophisticated and the boundary value problems become more complex, better descriptions of material behavior are required. In order to answer the question of how a material responds, we must begin to discover why the material responds as it does. It is no longer possible to rely solely on phenomenology to provide accurate relationships without regard to the physics taking place. This is particularly true for strongly nonlinear materials such as alluvium. The research described in this paper was conducted as a preliminary step to the formulation of a general constitutive law based only on micromechanical considerations. The purpose is to show how the properties of the individual components of the rock matrix affect the overall response.

The material of interest is a cemented, granular material. Presumably, this description could fit materials such as alluvium, sandstone and even granite where the strength and stiffness of the rock depend on the packing and structural characteristics of the grains and bonds.

Most continuum numerical models use some sort of plasticity to achieve nonlinear, inelastic behavior. The cap model, generalized by Sandler et al. (1976), has been extensively used to model both soil and rock. Since the formulation requires up to twenty-nine different curve-fitting parameters, laboratory data may be reproduced quite well. This model, unfortunately, gives no clue as to the internal processes taking place during deformation. Schatz (1976) reviews several theories for inelastic behavior in porous geologic media and makes a distinction between phenomenological and mechanistic formulations.

This paper will discuss the development and implementation of interparticle bonding into the distinct element method. Specific examples of

quasi-static and dynamic numerical experiments will be presented. The significance of the formation of multiple-particle clusters will be addressed in the context of observed macroscopic behavior. Finally, a summary will provide an overview and indicate where the research is going.

2 ASSUMPTIONS AND SIMPLIFICATIONS

The distinct element method is a numerical procedure for the analysis of assemblies of particles. Cundall and Strack (1979) describe how the code alternates between the application of a force-displacement law at each contact point and the equations of motion that translate and rotate each particle is space. The program used in this study was a two-dimensional version of the TRUBAL code, described by Cundall (1987). In two dimensions the translation and rotation of two particles may be resolved into three modes of relative motion shown in Figure 1 plus rigid body motion. It is assumed that the bonding material is linear and elastic and has boundaries parallel to the line connecting the particle centers. It is also assumed that all particles are of equal size although as will be shown later, particle clusters may have any arbitrary shape and size.

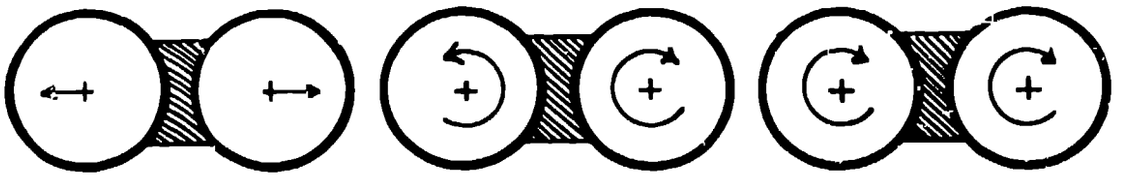

Figure 1. Three modes of relative deformation in two dimensions.

The present study was performed with bonds that were relatively weak with respect to the grains. This results in highly inelastic behavior at relatively low stress levels, typical of weakly cemented porous alluvium. Figure 2 is a scanning electron micrograph of Yuma Alluvium.

Figure 2. Photomicrograph of Yuma Alluvium from a depth of 14 m. Magnification is 480x.

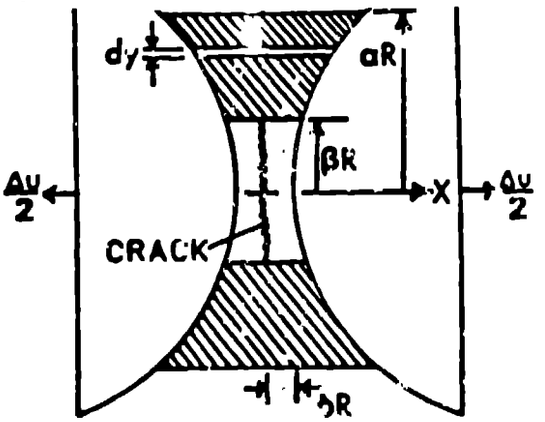

Figure 3. Assumed geometry and dimensionless constants for the interparticle bonding.

Notice the rounded shape of the particles and the orientation and shape of the bonds. This material is quite friable and is easily crushed by hand. These shapes are idealized with circles and straight line segments in the sections that follow.

2.1 The elastic restoring equations

Analytic expressions for the restoring forces and moments resulting from the motion shown in Figure 1 were incorporated into the distinct element code. Essentially, a special type of contact was defined and a second force-displacement law was invoked such that additional forces and moments were applied to particles that were bonded together. Each bond is defined by three dimensionless constants. The two disks shown in Figure 3 are cemented from y=-αR to +αR with a vertical, centered crack running from y=-βR to +βR. Only material above and below the crack contributes to the restoring forces. The particles are separated by a distance of 2δR. If E is the elastic (constrained) modulus and Δu is the imposed relative displacement, an expression for the relative stiffness may be obtained by integrating the stress-strain relation for a fiber over the length of the bond. If a = 1+δ, the relation in simple tension is:

$$(1) \qquad \frac{F/\Delta u}{E} = -w + \frac{a}{\sqrt{a^2 - 1}} \arccos\left(\frac{a\cos(w) - 1}{a - \cos(w)}\right) \qquad \begin{matrix} w=\arcsin(\alpha) \\ w=\arcsin(\beta) \end{matrix}.$$

Figure 4 shows the stiffness reduction as a function of crack length for different separation distances. Appropriate expressions were also obtained for the other two modes by Trent (1987) and Trent et al. (1987).

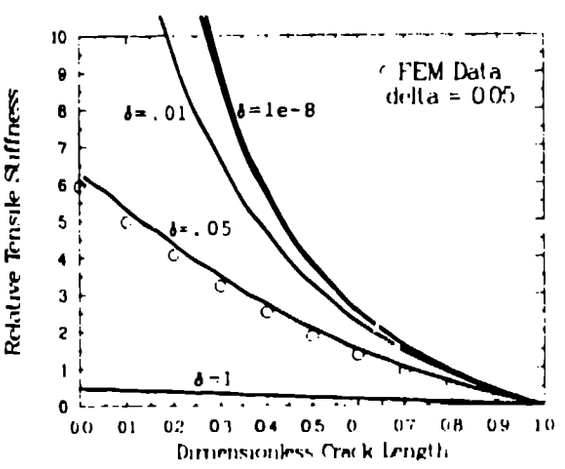

Figure 4. Relative stiffness in simple tension for 5 separations.

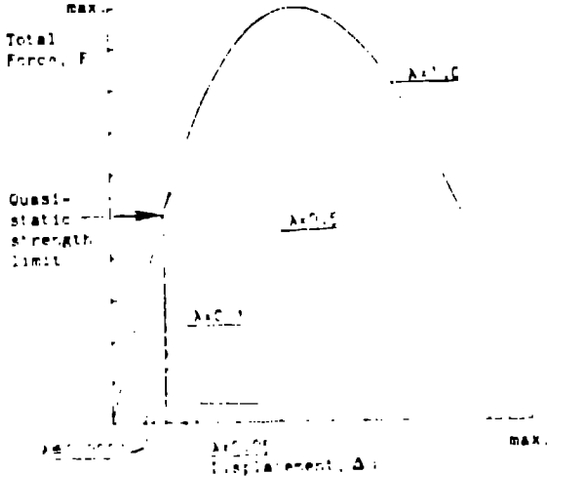

Figure 5. Force-displacement curves for one bond at 4 loading rates.

2.2 Bond fracture and crack growth

The code prescribes the strain during a timestep from the relative particle motion. Increasing tensile strain eventually leads to fracture. If the stress exceeds the tensile strength at the beginning of the timestep, fracture occurs. It is assumed that the crack grows at a constant rate, d. As the crack grows, the effective modulus of the bond decreases so the stress at the end of the timestep may or may not exceed the strength. The basis for this analysis is given by Margolin (1983).

The effective modulus is assumed to vary linearly with crack length,

$$(2) \qquad E_e = E_{max}(1 - \beta/\alpha),$$

which is nearly correct for δ greater than 0.05 as shown in Figure 4. The incremental strain and incremental stress are related by

$$(3) \qquad \Delta\varepsilon = \Delta\left(\sigma/E_e\right) = \frac{\sigma^{n+1}}{E_e^{n+1}} - \frac{\sigma^n}{E_e^n} .$$

If fracture growth continues during the entire timestep, Δt, at speed d, the ending stress can be evaluated using equations (2) and (3):

$$(4) \qquad \sigma^{n+1} = E_{max}\left(1 - \frac{\beta^n}{\alpha} - \frac{d\,\Delta t}{\alpha R}\right)\left(\Delta\varepsilon + \frac{\sigma^n}{E_e^n}\right) .$$

If σ^{n+1} exceeds the tensile strength, σ_t, the guess was correct and the growth is exactly d Δt. If it is less than σ_t then the crack arrested at some intermediate time and growth occurred only for some fraction of the timestep. If the initial stress is below σ_t then no crack growth occurs. However, the strain rate may force σ^{n+1} greater than σ_t resulting in crack initiation.

This procedure provides exact compatibility within a timestep between the imposed strain conditions and the modulus reduction which results from fracture at a finite rate. A stress criterion for failure was modified after Margolin (1984), incorporating additional tensile stress due to rolling and shear due to shearing rotations:

$$(5) \qquad \sigma_n^2 + \frac{\sigma_s^2}{2(1+\upsilon)} \geq \frac{\pi\, T\, E}{2(1-\upsilon^2)c}$$

where υ and E are the intact material Poisson's ratio and elastic modulus, respectively, and T is the energy required to build a new surface, a measurable material property. The crack radius (or length in one dimension) is defined by the variable, c. This is valid for quasi-static and dynamic loading. If the strain rate is high enough, stresses within the bonding will increase above the quasi-static value. This is shown in Figure 5 where force-displacement curves are shown for four different loading rates. The value $\lambda = v/d$ is the ratio of the particle velocity to the crack speed. If the loading rate is slow (or the crack propagation speed is fast) rupture is virtually instantaneous. For faster rates, very large internal forces can develop. The force-displacement relation for a single bond is shown in Figure 6. Notice unloading begins prior to complete fracture and the slope of the force-displacement curve after the crack stops growing is the effective modulus of the damaged material. Compressive response is equivalent to undamaged material.

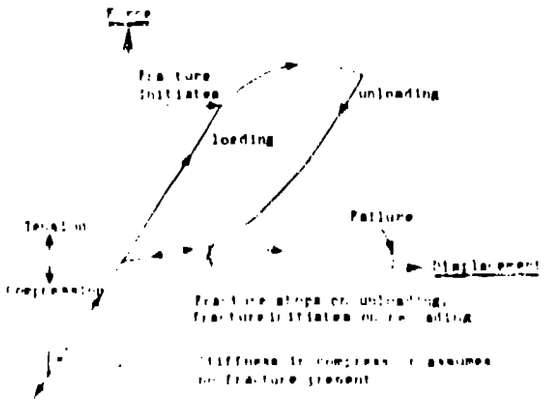

Figure 6. Force-displacement curve for loading, unloading and reloading.

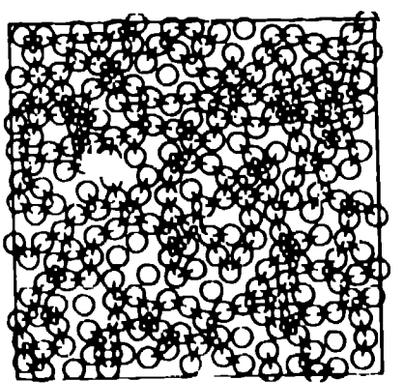

Figure 7. Initial distribution of bonded particles before loading.

3 QUASI-STATIC NUMERICAL EXPERIMENTS

The results of the quasi-static numerical experiments are given in terms of stress-strain relationships or pressure-volumetric compaction curves, much like the results of laboratory tests. The stress tensor must be adjusted due to the forces of the bonding on the particles. An analysis similar to Cundall and Strack (1983) was performed so that the average stress tensor is

$$(6) \qquad \bar{\sigma}_{ij} = \frac{1}{V} \sum_{p=1}^{N} \sum_{c=1}^{m} x_i^c F_j^c$$

where V is the sample volume, F_j is the force vector at particle contact (or bond) c, located at x_i, summed over all contacts (and bonds) m, for all particles, N. The stresses within the bonds add only a small correction since their volume is relatively insignificant.

3.1 Volumetric compaction

A random distribution of 244 particles was generated as illustrated in Figure 7. All particles closer than one-half radius were assumed to be bonded but the internal crack length (2BR) varied from 20 to 90% complete. The bond damage is reflected in the length of the line between particle centers. Figure 8 shows the pressure-volumetric strain data. This response is typical of alluvium, showing an initial elastic response followed by significant permanent volume reduction. Finally, the curve stiffens, reflecting the mineral constituents. The total pressure is the result of interparticle contacts and the forces exerted by the bonds. At first the pressure is due only to stresses in the bonds but as damage takes place and particles come into contact, the interparticle forces dominate the pressure. Figure 9 shows the final state. Bonds that are not completely fractured form distinct clusters of two or more particles, indicated by the numbers inside bonded grains.

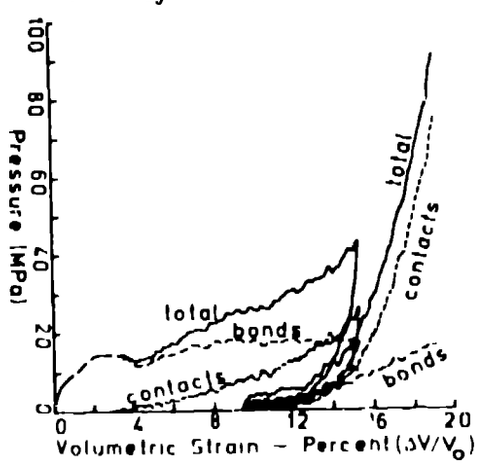

Figure 8. Pressure-volumetric strain curve showing the components.

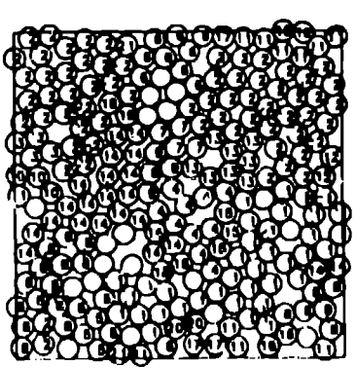

Figure 9. Final particle and bond distribution and cluster numbers.

3.2 Shear behavior

Two shearing experiments are presented here on samples similar to the distribution shown in Figure 7. The sample was first loaded to a moderate mean stress and then sheared by applying equal and opposite strain

rates to the periodic boundaries. The mean stress was maintained at a constant value by a numerical servo-control. The pressure-volumetric strain and shear stress-shear strain curves are shown in Figures 10 and 11. Notice the volume continues to decrease during shearing and the shear stress gradually increases and levels out to a residual value.

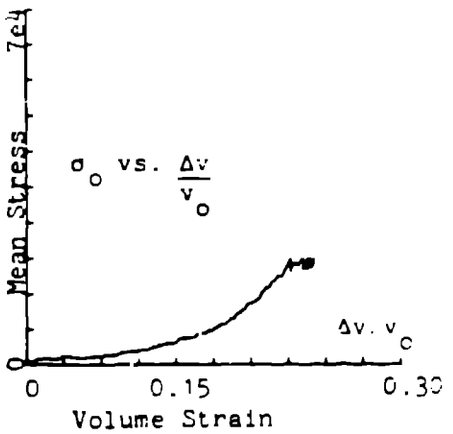

Figure 10. Pressure volume strain curve for compaction and shear.

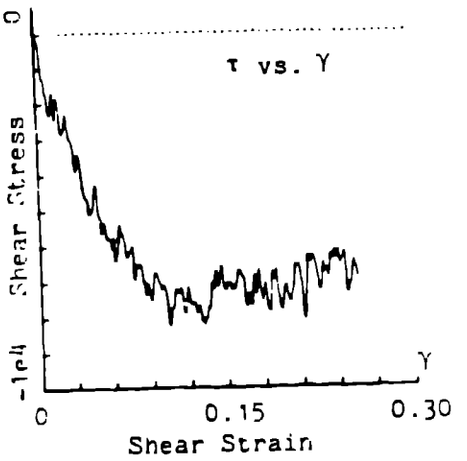

Figure 11. Shear stress-strain curve showing rise to residual strength.

The next test was identical to the first except the sample was over consolidated by applying a high confining pressure and then reducing the pressure to the same value as the previous case. The pressure and shear stress curves are shown in Figures 12 and 13, respectively. Here, volume expands in shear and the shear stress climbs to a peak value, 25% greater than the residual value in Figure 11 before dropping to this same level. This increase in strength and then softening behavior seems to be related to the orientation and distribution of multiple particle clusters formed during the over consolidation process. Overconsolidation had no effect on the shear strength for particles without bonding. More complete information on these tests is given by Trent (1987).

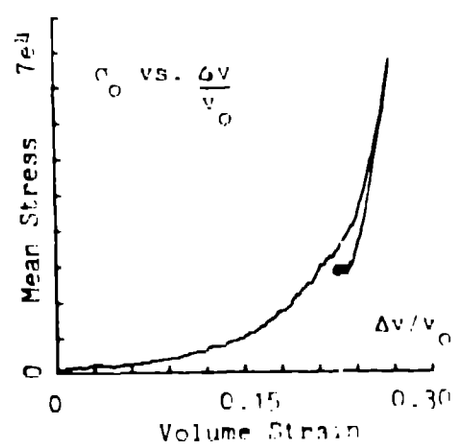

Figure 12. Pressure volume strain curve for overconsolidation, relaxation and shearing.

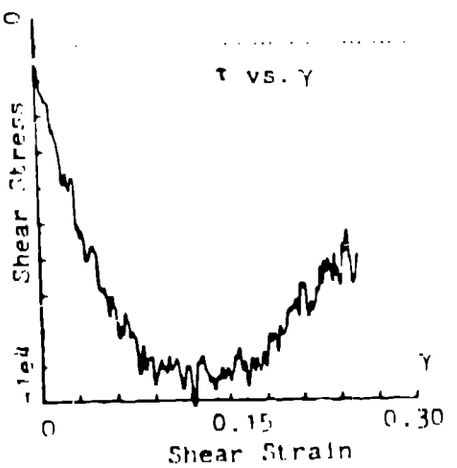

Figure 13. Shear stress-strain curve showing higher peak strength and softening to residual strength.

4 DYNAMIC NUMERICAL EXPERIMENTS

The failure criterion given in equation 6 is independent of strain rate and the formulation of the distinct element code is inherently dynamic. A random distribution of particles was generated by allowing new particles to settle on top of others. Figure 14 shows the initial distribution and six regions in which the average particle velocity is calculated. The particles were bonded together and then loaded by applying a constant downward (tensile) vertical velocity to the lowermost boundary of particles. Figure 15 shows this step function and the response in regions 2,3 and 6. Notice there is significant dispersion as the signal moves upward. The elastic modulus of the bonding material was increased by a factor of 15 and the same boundary condition applied. Figure 16 shows that the resulting wave is much stronger and sharper.

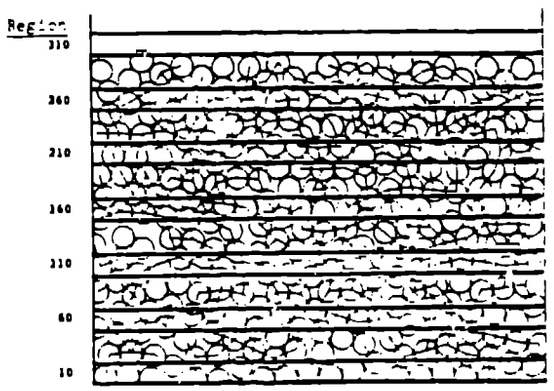

Figure 14. Random distribution of particles and averaging regions.

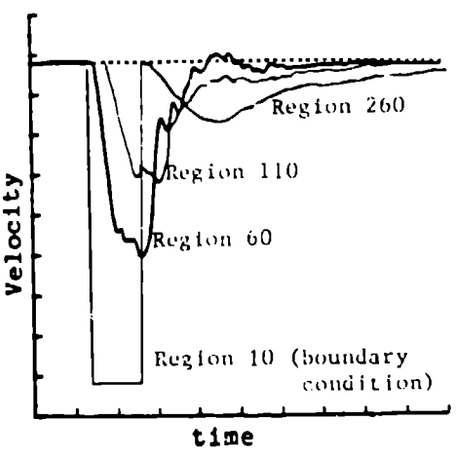

Figure 15. Velocity histories for soft bonds in regions 1,2,3 and 6.

The bonds in these two experiments were infinitely strong. If they are allowed to break. the signal is strongly affected. Figure 17 shows the average velocity histories in region 2 for strong, intermediate and weak bonds. These experiments show that a signal propagating through a bonded, porous medium is governed by the properties of the microstructure. Additional experiments and details are given by Trent (1987).

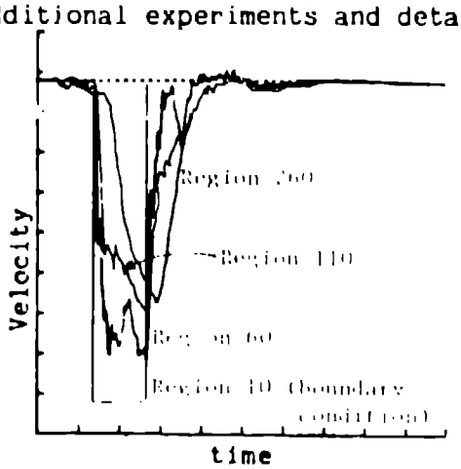

Figure 16. Velocity histories for regions 1,2,3 and 6 for bonds with high stiffnesses.

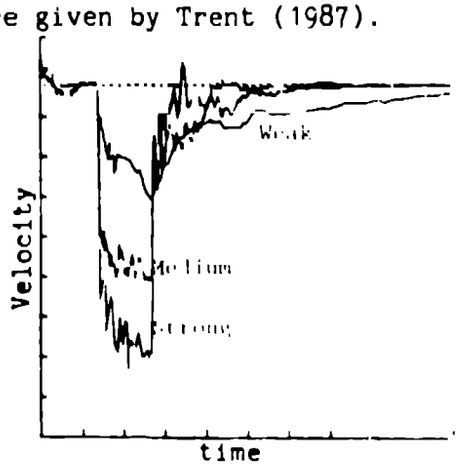

Figure 17. Velocity histories for region 2 showing the effect of bond strength.

5 SUMMARY AND CONCLUSIONS

The results of several numerical experiments have been presented and indicate that macroscopic phenomenology may be reproduced without the use of plasticity. A generalized Griffith criterion was used in both quasi-static and dynamic regimes as the only nonlinear failure mechanism. The formation and distribution of multiple particle clusters plays an important role in determining the shear strength of porous, weakly cemented granular material since the cluster distribution was significantly different and more compact after overconsolidation. The stiffness and strength of the individual bonds govern stress wave propagation characteristics in this type of material. Present research is directed toward the formulation of a general constitutive law that is based only on micromechanical considerations.

ACKNOWLEDGMENTS

I am most grateful for the many suggestions and reviews of this research by my thesis advisors, P.A. Cundall and L.G. Margolin. Funding was provided by the U.S. Department of Energy and the University of Minnesota.

REFERENCES

Cundall, P.A. 1987. Distinct element models of rock and soil structure. In E.T. Brown (ed.) Analytical and Computational Methods in Engineering Rock Mechanics, p.129-163. London: Allen & Unwin.

Cundall, P.A. & O.D.L. Strack 1979. A discrete numerical model for granular assemblies. Geotechnique 29:47-65.

Cundall, P.A. & O.D.L. Strack 1983. Modeling of microscopic mechanisms in granular material. In J.T. Jenkins & M. Satake (eds.) Mechanics of granular materials, p.137-149. Amsterdam: Elsevier.

Margolin, L.G. 1983. Elastic moduli of a cracked body. Int. J. Fracture 22:65-79.

Margolin, L.G. 1984. Generalized Griffith criterion for crack propagation. Eng. Fracture Mech. 19:539-543.

Sandler, I.S., F. Dimmagio & G.T. Baladi 1976. Generalized cap model for geologic materials. J. Geotech. Div. A.S.C.E. 102:683-699.

Schatz, J.F. 1976. Models of inelastic volume deformation for porous geologic materials. In S. Cowin & M. Carroll (eds.) The effects of voids on material deformation, p.141-170. New York: Am. Soc. Mech. Eng.

Trent, B.C. The effect of micro-structure on the macroscopic behavior of cemented granular material. Ph.D. thesis, University of Minnesota, Minneapolis, Minnesota.

Trent, B.C., L.G. Margolin, P.A. Cundall & E.S. Gaffney 1987. The micromechanics of cemented granular material. In C.S. Desai et al. (eds.) Constitutive laws for engineering materials: theory and application, p.795-802. New York: Elsevier.